Available online at www.sciencedirect.com
ScienceDirect
Journal of the European Ceramic Society 29 (2009) 1735–1741
www.elsevier.com/locate/jeurceramsoc

Doping behaviors of dysprosium, yttrium and holmium in $BaTiO_3$ ceramics

Kum-Jin Park [a], Chang-Hoon Kim [a,*], Yeo-Joo Yoon [b], Soon-Mo Song [a], Young-Tae Kim [a], Kang-Heon Hur [c]

[a] *Material Development Group, LCR Division, Samsung Electro-Mechanics, Suwon, Republic of Korea*
[b] *Analytical Research Group, Central R&D Institute, Samsung Electro-Mechanics, Suwon, Republic of Korea*
[c] *LCR Development Team, LCR Division, Samsung Electro-Mechanics, Suwon, Republic of Korea*

Received 10 July 2008; received in revised form 9 October 2008; accepted 24 October 2008
Available online 20 December 2008

Abstract

The difference in doping behaviors of intermediate rare-earth ions and their effects on the dielectric property and microstructure of $BaTiO_3$(BT)–MgO–Re_2O_3 (Re = Dy, Ho, Y) system were investigated. Compared to Y and Ho, Dy ions provided BT ceramics with a high rate of densification and much enhanced shell formation due to their high solubility in BT. However, the microstructure of the Dy doped specimen was unstable at high temperatures in terms of grain growth. Until the specimen was densified, the tetragonality of Dy doped specimen was remarkably decreased and the substitution amount of Dy ions for A-site was larger than that of Y and Ho ions. After complete densification, the tetragonality was increased again and the B-site incorporation of Dy ions was increased far more than that of Y and Ho ions resulting in grain growth. This different behavior was considered to result in temperature coefficient of capacitance curves in the Dy doped specimen different from that of typical core–shell grains.

Keywords: D. $BaTiO_3$; A. Sintering; Rare-earth; Doping

1. Introduction

Recently, the production process of multilayer ceramic capacitors (MLCCs) has been dramatically improved to meet the demands for higher capacitance achieved in a smaller chip consisting of several hundreds of dielectric layers of 1 μm or less in thickness. In order to form 1-μm thick layers and meet the X5R (the tolerance of capacitance in −55 to +85 °C is ±15%) or X7R (the tolerance of capacitance in −55 to +125 °C is ±15%) specifications, $BaTiO_3$ (BT) grains need to be small and form a so-called core–shell structure. In the core–shell structure, the additive elements are partially dissolved in the BT lattice to form a shell which surrounds the core region. The shell is known to have non-ferroelectric pseudo-cubic structure, whereas the core is pure BT with a ferroelectric tetragonal structure.[1–3]

It is reported that a rare-earth element is a dominant additive in forming a shell and the core–shell structure is well developed when the rare-earth element and magnesium are added to BT.[4] Rare-earth elements are known to exhibit useful functions of stabilizing the temperature dependence of relative dielectric constant and lowering the dissipation factor in dielectric ceramics.[5,6] As a result, the dielectric performance of the capacitors would be influenced by the amount and kind of rare-earth element. When the dopants are incorporated into the BT lattice, the substitutional chemistry is determined by strain, charge, charge-distribution and ionic size.[7] There have been many reports that the ionic size is a main factor influencing the incorporation of rare-earth ions into BT ceramics.[7–12] Table 1 shows ionic radii of Ba, Ti, Mg and rare-earth elements, in which the ionic radii of rare-earth elements in 12 coordination were obtained by extrapolation from the relationship between the coordination number and the ionic radius.[13] Assuming that the local strain is similar in both A- and B-sites, small rare-earth ions will occupy the B-site and large ones the A-site, whereas the intermediate ions will occupy both sites with different partitioning for each ion.[8,9]

* Corresponding author.
E-mail address: ch1221.kim@samsung.com (C.-H. Kim).

0955-2219/$ – see front matter © 2008 Elsevier Ltd. All rights reserved.
doi:10.1016/j.jeurceramsoc.2008.10.021

Table 1
Effective ionic radii of various elements.[13]

Ion	Ionic radius (Å)	
	6 coordination (B-site)	12 coordination (A-site)
Ba^{2+}		1.610
Ti^{4+}	0.605	
Mg^{2+}	0.720	
Dy^{3+}	0.912	1.255
Ho^{3+}	0.901	1.234
Y^{3+}	0.900	1.234

The rare-earth elements are known to act as a donor when they dissolve in A-site and an acceptor in B-site.

MLCCs are usually sintered in a reducing atmosphere to prevent Ni electrodes from oxidation, so that electrons are generated by the formation of doubly ionized oxygen vacancies in a low oxygen partial pressure. The introduction of acceptors to BT has an effect of compensating positively charged oxygen vacancies and thus suppressing the generation of electrons. Thus, the acceptor concentration needs to be higher than the electron defect concentration to keep BT insulating.[14] Since the concentrations of electronic defects in acceptor or donor doped BT are dependent on the sintering atmosphere as well as on the dopant amount, it is difficult to optimize the concentration of acceptor or donor.[15,16] The amphoteric rare-earth ion, however, help balance between donor and acceptor, so the reliability of MLCCs would be improved by its introduction. It is reported that the amphoteric rare-earth ions of intermediate ionic radius, such as Dy, Y and Ho, provide BT ceramics with good electrical properties and a high reliability.[5,6] In particular, the electrical performance and related reliability of the capacitor are attributed to the solubility, distribution and site occupation of rare-earth ions.[5,12] It is also reported that the solid solubilities of Dy, Ho, and Y in the BT structure are similar due to their similar ionic size.[17]

The purpose of this study is to study the difference in doping behaviors of intermediate rare-earth elements, i.e., Dy, Y and Ho, which have similar ionic size and the resulting effect on the microstructures of BT ceramics, although they are known to have similar solubilities in BT lattice. The specimens were prepared with the addition of Dy, Y, Ho and Mg, and their microstructures and dielectric properties were investigated.

2. Experimental procedure

Hydrothermally synthesized BT powders (Samsung Fine Chemicals) were weighed with Dy_2O_3 (Shinetsu), Y_2O_3 (Shinetsu), Ho_2O_3 (Shinetsu), MgO (Ube Materials), $BaCO_3$ (Sakai), and SiO_2 (AEROSIL) powders according to the composition in Table 2. MgO were added in the same amount to facilitate shell formation with the rare-earth elements. The $BaCO_3$ and SiO_2 were added to aid sintering of $BaTiO_3$ by reducing its sintering temperature. Thus, the kind of intermediate rare-earth element was varied in this study.

The powders were ball-milled in solvent (ethanol and toluene) with dispersant for 5 h and mixed with BM-2 PVB binder (Sekisui) for 15 h. Green sheets were formed by doctor blade casting of the powder slurry on PET film. Then, the sheets were laminated, pressed and cut into square-shaped plates of 1-mm thickness. To mimic the process for a base-metal electrode MLCC, the plates were baked for binder burn out and sintered at various temperatures (1190–1350 °C) in a reducing atmosphere (PO_2 of 10^{-9} atm), followed by re-oxidation at 1000 °C in N_2/O_2 atmosphere (25 ppm O_2).

Bulk density of the sintered specimen was measured using Archimedes method, and the surfaces of bulk specimens were observed by scanning electron microscope (SEM, LEICA S440) to examine the grain size distribution. For a detailed study of microstructure, electron transparent samples were prepared by tripod polishing of the sintered specimen followed by ion beam thinning (Gatan PIPS), and investigated using transmission electron microscope (TEM, FEI G2 F20) operating at 200 kV. The composition profiles of dopants particularly in core–shell structured grains were analyzed using TEM energy dispersive spectroscopy (EDS) by choosing an appropriate electron beam probe size. The core and shell regions within a grain were distinguished through TEM imaging and EDS analysis, and grain radius and shell width were measured.

Crystal structure was studied by X-ray diffractometry (XRD, Rigaku RINT2200 HF) on pulverized bulk specimens in 2θ range of 10–130° at 0.01° step, 4 s/step. Rietveld refinement was performed to obtain the lattice parameters of the specimen.[18]

The capacitance of the sintered specimen with In–Ga paste on both surfaces was measured in the temperature range of −25 to 150 °C at 1 kHz, 1 Vrms using an Agilent 4284A precision LCR meter.

3. Results and discussion

3.1. Densification and grain growth behavior

Fig. 1 shows the change of bulk density of rare-earth doped BT ceramics sintered at various temperatures. The density of Dy doped specimen reached at saturation the earliest whereas the Y or Ho doped specimen showed a low rate of densification. It is known that additive components such as rare-earth element and

Table 2
Composition of specimens.

Specimen	$BaTiO_3$	Dy_2O_3	Y_2O_3	Ho_2O_3	MgO	$BaCO_3$	SiO_2
Dy doped	100	2	0	0	2	1	1.5
Y doped	100	0	2	0	2	1	1.5
Ho doped	100	0	0	2	2	1	1.5
Undoped	100	0	0	0	0	1	1.5

All numbers are in moles.

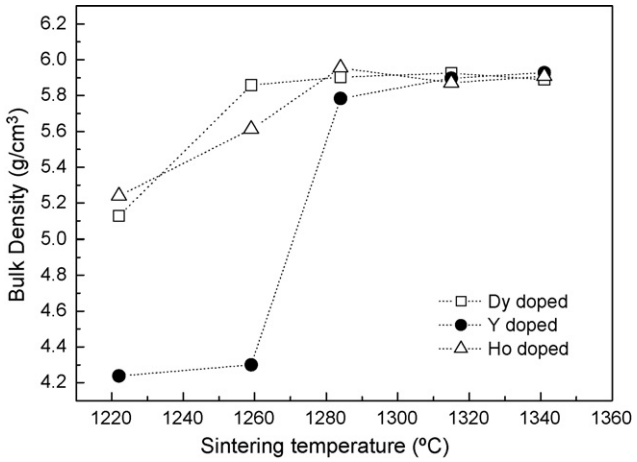

Fig. 1. Bulk density of rare-earth doped BT specimens as a function of sintering temperature.

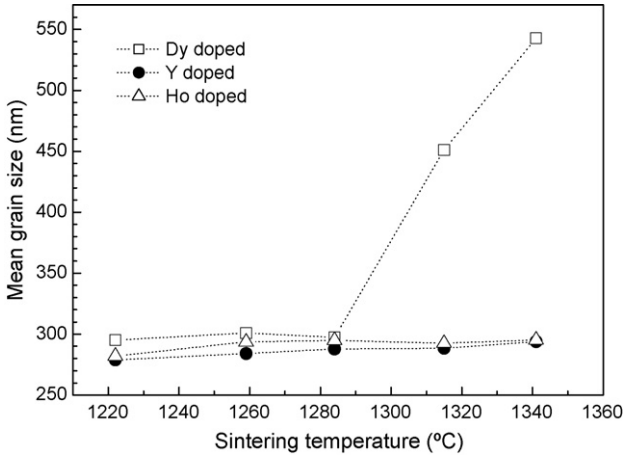

Fig. 3. Mean grain size of rare-earth doped BT specimens sintered at various temperatures.

Mg suppressed necking of BT grains due to the reduced grain boundary mobility, and then hindered the densification.[19,20] The result of bulk density measurement in Fig. 1 indicates that the Dy could not effectively prevent the densification of BT grains compared to Y and Ho. Consequently, it is considered that Dy ions dissolved easily in the BT lattice than Y and Ho ions, leading to a higher densification rate in Dy doped specimen.

Fig. 2 shows SEM images of the specimens after the densification was completed. The undoped specimen exhibited grains grown over several tens of micrometers. The grain size of rare-earth doped specimens was much smaller than that of undoped specimen, but the Dy doped specimen sintered at 1315 °C had larger grains than Y and Ho doped specimens sintered at 1341 °C. The mean grain sizes measured from SEM images of each specimen as a function of sintering temperature were plotted in Fig. 3. Y and Ho doped specimens showed almost no grain growth over the whole temperature range. In the Dy doped specimen, the mean grain size did not show any difference until 1284 °C, but above the temperature of maximum density, the grains grew remarkably with an increase in sintering temperature.

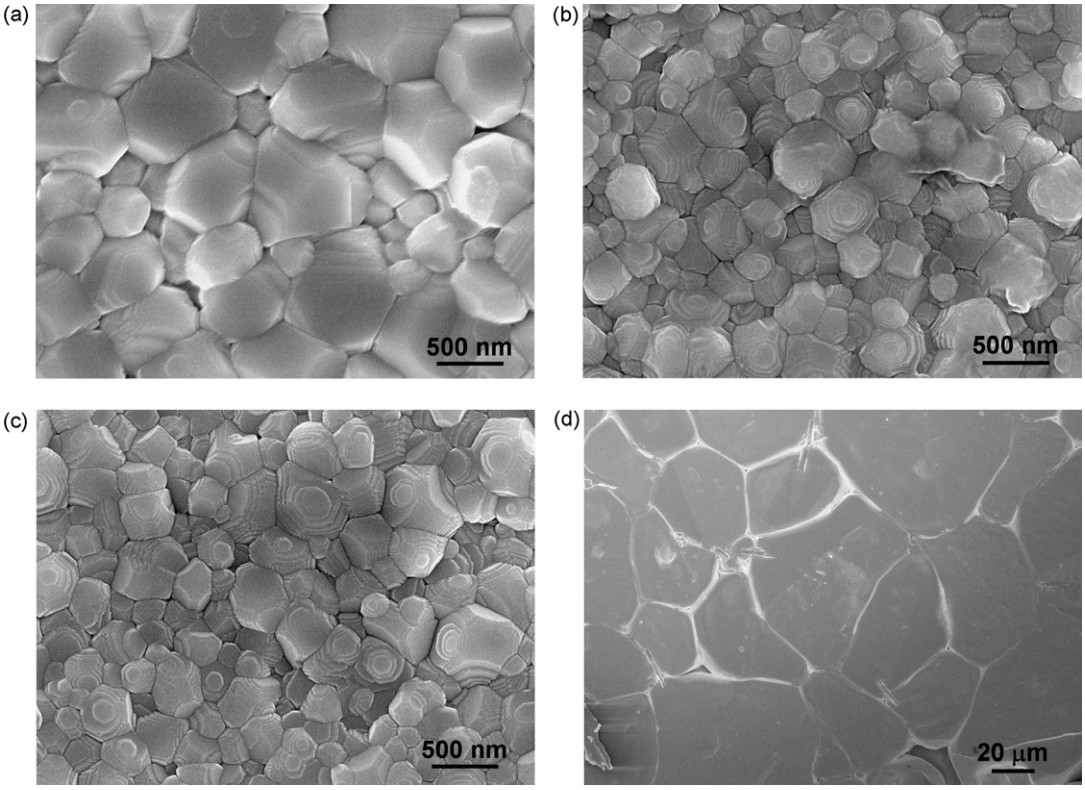

Fig. 2. Scanning electron micrographs of the surfaces of rare-earth doped BT specimens: (a) Dy-doped specimen sintered at 1315 °C, (b) Y-doped at 1341 °C, (c) Ho-doped at 1341 °C, and (d) undoped at 1284 °C.

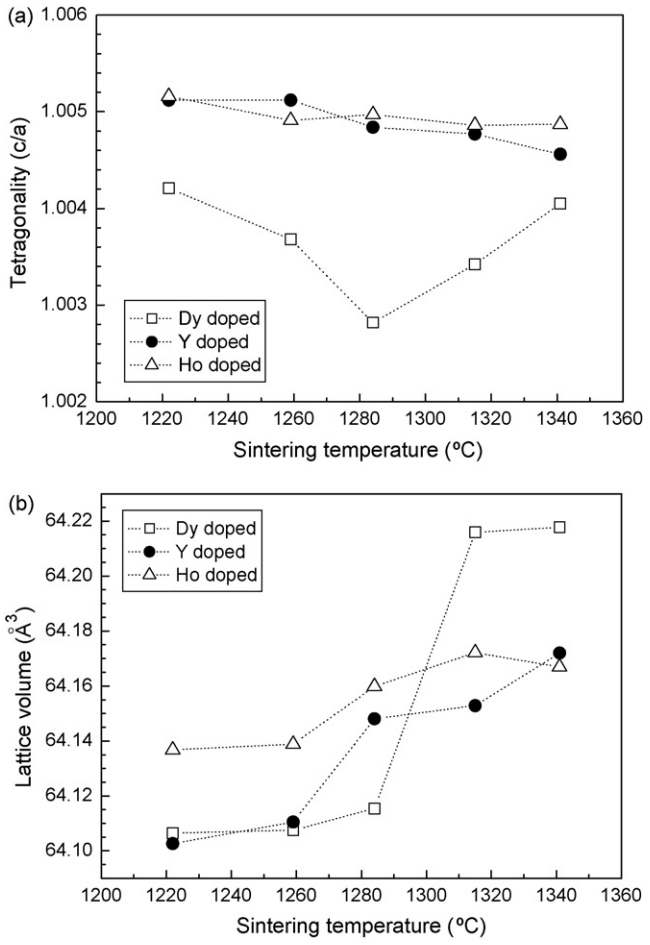

Fig. 4. (a) Tetragonality (*c*/*a*) and (b) lattice volume of rare-earth doped BT specimens as a function of sintering temperature.

Fig. 4 shows the results of XRD analysis of the rare-earth doped specimens. Since the shell with pseudo-cubic structure is formed by dissolution of dopants in BT lattice, the tetragonality (*c*/*a*) of the specimen was decreased as the incorporation of rare-earth elements increased (Fig. 4(a)). In Y and Ho doped specimens, the tetragonality slightly decreased with the increase in sintering temperature, which indicated that the amount of Y and Ho ions dissolved in BT did not much increase with the sintering temperature. On the other hand, the tetragonality of Dy doped specimen decreased remarkably until 1284 °C, and then increased again on further increase of sintering temperature. The tetragonality turned to increase at the temperature when the grain growth occurred. The increase of tetragonality as well as the grain growth in Dy doped specimen is not clearly understood, which is subject to further studies. Fig. 4(b) shows the change of lattice volume of rare-earth doped specimens. The lattice volume was increased with the increase in sintering temperature. Since the intermediate rare-earth ions are smaller than Ba and larger than Ti, their substitution for A-site and B-site would lead to a decrease and increase in the lattice volume, respectively.[12,21–23] It is reported that during the incorporation of rare-earth ion with the valence of 3+, A-site drives it towards a lower valence while B-site towards a higher valence, and that higher temperature drives the ions towards a higher valence.[7] Consequently, the result in Fig. 4(b) indicates that the incorporation of rare-earth ions into B-site was enhanced as the sintering temperature increased. In addition, Fig. 4(b) showed that before the densification was completed, the lattice volume of Dy doped specimen was smaller than that of Y or Ho doped specimens. Since the radius of Dy ion is slightly larger than that of Y or Ho ions, the lattice volume of Dy doped specimen might have been slightly larger with the same amount of incorporation of the dopant. However, the smaller *c*/*a* value and the smaller lattice volume in the Dy doped specimen shown in Fig. 4 implied that the amount of Dy ion substitution for A-site is larger than that of Y and Ho ions until the specimen was fully densified.

Above 1284 °C, the lattice volume of Dy doped specimen greatly increased with sintering temperature accompanied by grain growth, whereas the lattice volume of Y and Ho doped specimens did not change much. It indicates that after the completion of densification Dy ions continued to be incorporated into BT lattice, and that the B-site incorporation of Dy ions took place far more compared to Y and Ho ions. As a result of B-site incorporation, Ti ions could come out of shell region to grain boundary. In the TEM investigation on the Dy doped specimen sintered at 1341 °C, the local Ti concentration within the BT grain was measured by electron energy loss spectrometry (EELS) analysis as shown in Fig. 5. The intensity ratio of Ti–$L_{2,3}$ edge to Ba–$M_{4,5}$ edge was calculated to be 1.68 and 1.46 for core and shell region, respectively. Though the difficulty in obtaining the absolute Ti to Ba mol ratio, it is reasonable to compare the relative composition in the same specimen, and it seems like that the Dy substitution for B-site in the shell region could result in shift of Ti ions from shell to grain boundary. Since the excess Ti at grain boundary is known to easily form a eutectic liquid phase,[24,25] the grain growth in the Dy doped specimen sintered at high temperatures could be attributed to enhanced Dy substitution for B-site.

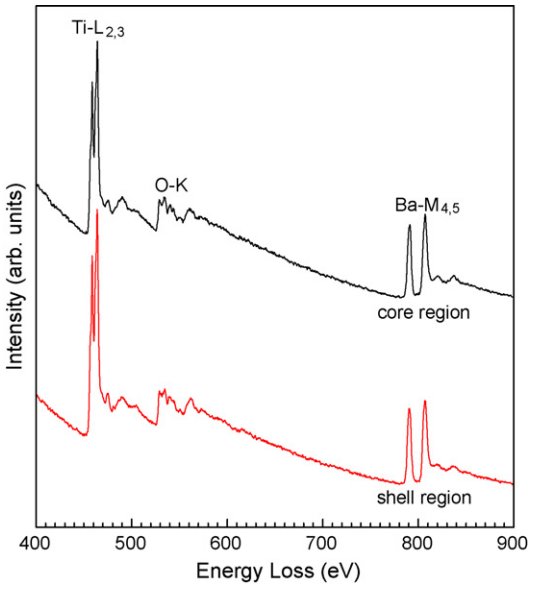

Fig. 5. TEM EELS spectra of Ti-$L_{2,3}$, O-*K* and Ba-$M_{4,5}$ edges for core and shell regions within a grain in Dy doped specimen sintered at 1341 °C.

In case of rare-earth ions which can incorporate into both sites, it is reported that at first, they preferentially occupy A-site, and then occupy B-site as the substitution increases.[21–23] From the various microstructural investigations, the Dy ion seems to more easily substitute for BT lattice than Y and Ho ions in spite of their similar ionic sizes. The high rate of densification and significant reduction of tetragonality in the Dy doped specimen indicated that Dy could more readily incorporate into A-site while the enhanced grain growth was attributed to its larger substitution for B-site compared to Y and Ho.

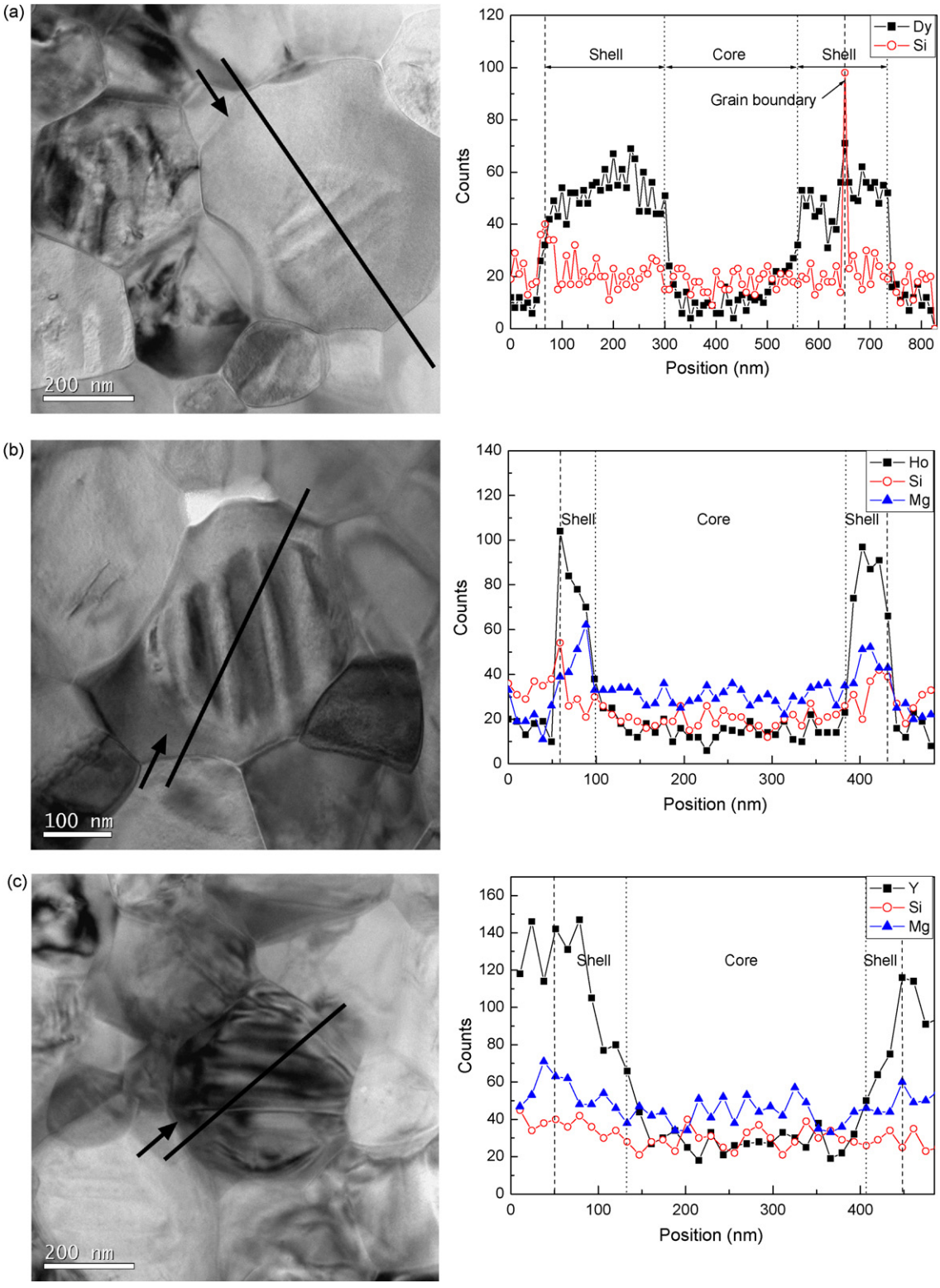

Fig. 6. TEM bright field image and EDS line profile for a typical core–shell grain: (a) Dy doped and (b) Ho doped specimens sintered at 1284 °C, and (c) Y doped specimen sintered at 1315 °C.

3.2. Core–shell structure

TEM investigation was carried out on Dy and Ho doped specimens sintered at 1284 °C, and Y doped specimen sintered at 1315 °C; the Y doped specimen at 1315 °C was selected due to the incompletion of densification at 1284 °C. Fig. 6 shows the microstructures and the results of EDS composition analysis for core–shell grains in each specimen. The concentrations of rare-earth ions were preserved to a certain depth from the grain boundary and decreased toward the core region. The concentration gradients of Mg and Si were not clearly observed across the shell-to-core boundary. Since the position of Mg Kα peak (1.254 keV) in EDS spectrum is very close to that of Dy Mα peak (1.293 keV), the EDS analysis of Mg was not carried out in Dy doped specimen. The grain boundary phase was occasionally observed in all specimens, and the EDS analysis detected high intensity of Si at the grain boundary as pointed out in Fig. 6(a). The ratio of shell width to grain radius was measured in each specimen. The shell width can be overestimated in TEM images because of partial overlapping of adjacent grains inside of the TEM sample, but the sample-to-sample comparison is reasonable. The Dy doped specimen showed a higher fraction of shell in the dielectric grain than the Y and Ho doped specimens. This result is correspondent to the fact that the Dy ions diffused more easily into BT lattice than Y and Ho ions as confirmed by XRD analysis. In addition, the discontinuity of shell formation in the Dy doped specimen was smaller that in Y and Ho doped specimens. The TEM investigation revealed that the Dy doped specimen had more developed and more uniform core–shell grains compared to Y and Ho doped specimens.

Fig. 7 shows temperature coefficient of capacitance (TCC) vs. temperature curves of the specimens as a function of sintering temperature. The undoped specimen showed a curve typical to BT ceramic, exhibiting a sharp peak at Curie temperature ($T_c \approx 130$ °C) and a shallow peak associated with the orthorhombic–tetragonal transition at about 25 °C. The peak at T_c was increased with the increase in sintering temperature, which resulted from grain growth. In the core–shell structured grain, the shell consists of a series of different phases according to their additive concentrations dissolved in BT lattice. The superposition of the individual phase transitions results in rather diffuse TCC curve, which then makes the TCC curve less dependent on the temperature change.[26,27] The TCC curves of Y and Ho doped specimens were much more stable than that of undoped specimen; a quite shallow peak at T_c, and little change as a function of sintering temperature (Fig. 6(c) and (d)). The TCC curve of Dy doped specimen was similar to those of Y and Ho doped specimens until the sintering temperature reached 1284 °C. However, the specimen sintered at higher temperatures showing grain growth exhibited a different behavior; a broad peak at about 70 °C (TCC max temperature, T_m) as shown Fig. 7(b). In contrast to the undoped specimen, the Dy doped

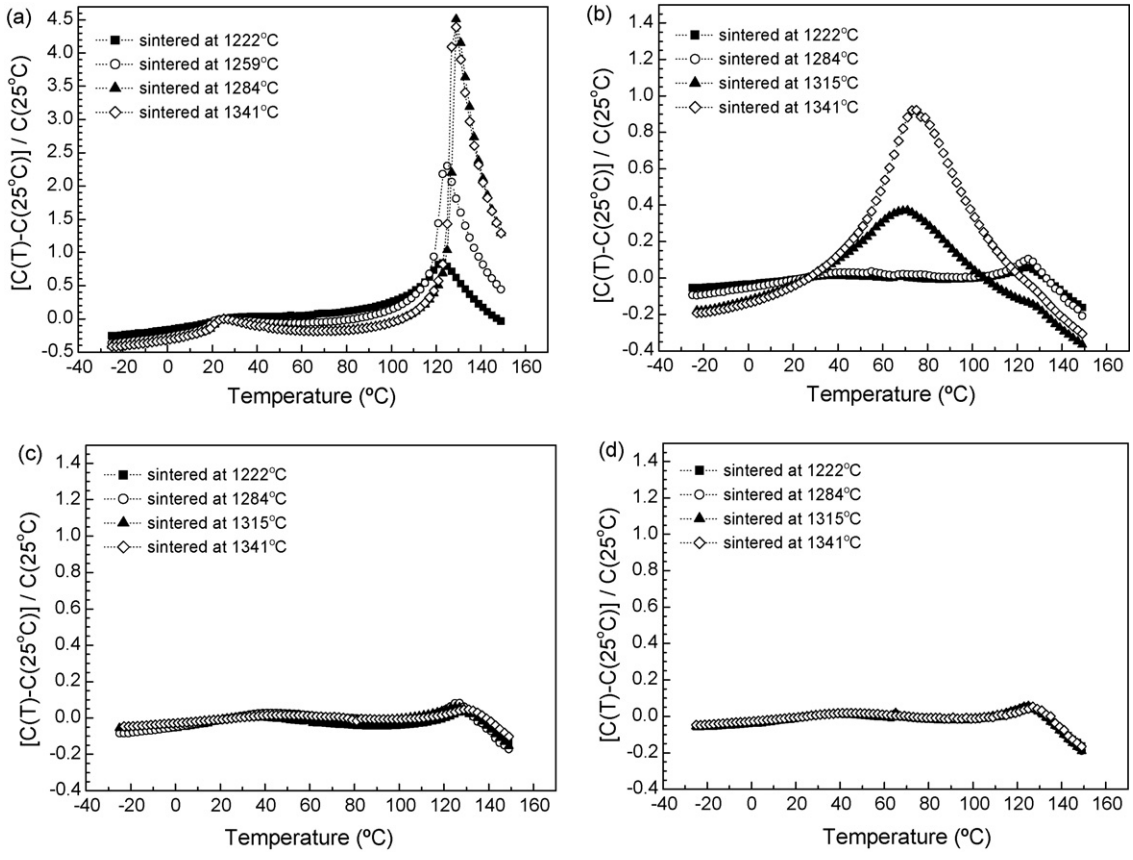

Fig. 7. Temperature coefficient of capacitance curves of the specimens as a function of sintering temperature; (a) undoped, (b) Dy doped, (c) Y doped, and (d) Ho doped.

specimen showed that the peak at T_c decreased, but the peak at T_m increased with increasing grain size. It is considered that the peaks at T_c and T_m correspond to core and shell region, respectively. The incorporation of Dy into B-site was continuously increased and the grains grew with much expanded shell region which might have characteristics of relaxor.[28] For this reason, TCC curve of the Dy doped specimen sintered above 1284 °C behaved differently from that of specimen with typical core–shell grains.

4. Conclusions

The difference in doping behaviors of rare-earth ions with intermediate ionic size and their effects on the dielectric property and the microstructure of BT-MgO–Re_2O_3 (Re = Dy, Ho, Y) system were investigated. Compared to Y and Ho ions, Dy ions provided BT ceramics with a high rate of densification and much enhanced shell formation due to their high solubility. However, the microstructure of the Dy doped specimen was unstable at high temperatures unlike Y and Ho doped specimens. Until the sintering temperature was reached at 1284 °C, the tetragonality of Dy doped specimen was remarkably decreased and the substitution amount of Dy ions for A-site was larger than that of Y and Ho ions. Above that temperature, the tetragonality was increased again and the B-site incorporation of Dy ions was increased far more than that of Y and Ho ions resulting in grain growth. While the Y and Ho doped specimens exhibited TCC curves insensitive to temperature change, the Dy doped specimen showed a different behavior corresponding to grain growth with enhanced B-site incorporation.

References

1. Randall, C. A., Wang, S. F., Laubscher, D., Dougherty, J. P. and Huebner, W., Structure property relationships in core–shell $BaTiO_3$–LiF ceramics. *J. Mater. Res.*, 1993, **8**, 871–879.
2. Yoon, S. H., Lee, J. H., Kim, D. Y. and Hwang, N. M., Core–shell structure of acceptor-rich, coarse barium titanate grains. *J. Am. Ceram. Soc.*, 2002, **85**, 3111–3113.
3. Fujikawa, Y., Umeda, Y. and Yamane, F., Analysis on the sintering process of X7R MLCC materials. *J. Jpn. Soc. Powder Powder Metall.*, 2004, **51**, 839–844.
4. Kim, C. H., Park, K. J., Yoon, Y. J., Hong, M. H., Hong, J. O. and Hur, K. H., Role of yttrium and magnesium in the formation of core–shell structure of $BaTiO_3$ grains in MLCC. *J. Eur. Ceram. Soc.*, 2008, **28**, 1213–1219.
5. Sakabe, Y., Hamaji, Y., Sano, H. and Wada, N., Effects of rare-earth oxides on the reliability of X7R dielectrics. *Jpn. J. Appl. Phys.*, 2002, **41**, 5668–5679.
6. Saito, H., Chazono, H., Kishi, H. and Yamaoka, N., X7R Multilayer ceramic capacitors with nickel electrodes. *Jpn. J. Appl. Phys.*, 2001, **30**, 2307–2310.
7. Tsur, Y., Dunbar, T. D. and Randall, C. A., Crystal and defect chemistry of rare-earth cations in $BaTiO_3$. *J. Electroceram.*, 2001, **7**, 25–34.
8. Lewis, G. V. and Catlow, C. R. A., Computer modeling of barium titanate. *Radiat. Effects*, 1983, **73**, 307–314.
9. Lewis, G. V. and Catlow, C. R. A., Deffect studies of doped and undoped barium titanate using computer simulation techniques. *J. Phys. Chem. Sol.*, 1986, **47**, 89–97.
10. Tsur, Y., Hitomi, A., Scrymgeour, I. and Randall, C. A., Site occupancy of rare-earth cations in $BaTiO_3$. *Jpn. J. Appl. Phys.*, 2001, **40**, 255–258.
11. Kishi, H., Mizuno, Y. and Chazono, H., Base-metal electrode-multilayer ceramics capacitors: past, present and future perspectives. *Jpn. J. Appl. Phys.*, 2003, **42**, 1–15.
12. Kishi, H., Kohzu, N., Sugino, J., Ohsato, H., Iguchi, Y. and Okuda, T., The effect of rare-earth (La, Sm, Dy, Ho and Er) and Mg on the microstructure in $BaTiO_3$. *J. Eur. Ceram. Soc.*, 1999, **19**, 1043–1046.
13. Shannon, R. D., Revised effective ionic radii and systematic studies of interatomic distances in halides and chalcogenides. *Acta Crystallogr. A*, 1976, **32**, 751–767.
14. Yoon, S. H., Hong, M. H., Hong, J. O., Kim, Y. T. and Hur, K. H., Effect of acceptor (Mg) concentration on the electrical resistance at room and high (200 °C) temperatures of acceptor (Mg)-doped $BaTiO_3$ ceramics. *J. Appl. Phys.*, 2007, **102**, 054105.
15. Sasaki, K. and Maier, J., Low-temperature defect chemistry of oxides. I. General aspects and numerical calculations. *J. Appl. Phys.*, 1999, **86**, 5422–5433.
16. Yoon, S. H. and Kim, H., Effect of donor (Nb) concentration on the bulk electrical resistivity of Nb-doped barium titanate. *J. Appl. Phys.*, 2002, **92**, 1039–1047.
17. Makovec, D., Samardzija, Z. and Drofenik, M., Solid solubility of holmium, yttrium, dysprosium in $BaTiO_3$. *J. Am. Ceram. Soc.*, 2004, **87**, 1324–1329.
18. Cullity, B. D., *Elements of X-ray Diffraction*. Addison-Wesley, London, 1978, pp. 281–292.
19. Lu, H. Y. and Lin, M. H., Charge compensation mechanism in yttria-doped barium titanate. *Ceram. Int.*, 2005, **31**, 989–997.
20. Andrei, K., Tomoya, H., Hiroshi, K. and Hitoshi, O., Effect of Ho/Mg ratio on formation of core–shell structure in $BaTiO_3$ and on dielectric properties of $BaTiO_3$ ceramics. *Jpn. J. Appl. Phys.*, 2002, **41**, 6934–6937.
21. Miao, H., Dong, M., Tan, G. and Pu, Y., Doping effects of Dy and Mg on $BaTiO_3$ ceramics prepared by hydrothermal method. *J. Electroceram.*, 2006, **16**, 297–300.
22. Kim, J. H., Yoon, S. H. and Han, Y. H., Effects of Y_2O_3 addition on electrical conductivity and dielectric properties of Ba-excess $BaTiO_3$. *J. Eur. Ceram. Soc.*, 2007, **27**, 1113–1116.
23. Kishi, H., Kohzu, N., Iguchi, Y., Sugino, J., Kato, M., Ohsato, H. and Okuda, T., Occupational sites and dielectric properties of rare-earth and Mn substituted $BaTiO_3$. *J. Eur. Ceram. Soc.*, 2001, **21**, 1643–1647.
24. Lee, J. K., Hong, K. S. and Jang, J. W., Roles of Ba/Ti ratios in the dielectric properties of $BaTiO_3$ ceramics. *J. Am. Ceram. Soc.*, 2001, **84**, 2001–2006.
25. Yoo, Y. S., Kim, J. J. and Kim, D. Y., Effects of heating rate on the microstructural evolution during sintering of $BaTiO_3$ ceramics. *J. Am. Ceram. Soc.*, 1987, **70**, C322–C324.
26. McCauley, D. E., Chu, M. S. H. and Megherhi, M. H., Po_2 dependence of the diffuse-phase transition in base metal capacitor dielectrics. *J. Am. Ceram. Soc.*, 2006, **89**, 193–201.
27. Liu, X., Cheng, S. and Randall, C. A., The core–shell structure in ultrafine X7R dielectric ceramics. *J. Kor. Phys. Soc.*, 1998, **32**, S312–S315.
28. Samara, G. A., The relaxational properties of compositionally disordered ABO_3 perovskites. *J. Phys.: Condens. Mater.*, 2003, **15**, R367–R411.